# Single-ended Time Domain Fault Location Based on Transient Signal Measurements of Transmission Lines

Jian Luo, *Member*, *IEEE*, Yao Liu, Qiushi Cui, *Member*, *IEEE*, Jiayong Zhong, *Member*, *IEEE*, and Lin Zhang

***Abstract*—Precise fault location plays an important role in the reliability of modern power systems. With the increasing penetration of renewable energy sources, the power system experiences a decrease in system inertia and alterations in steady-state characteristics following a fault occurrence. Most existing single-ended phasor domain methods assume a certain impedance of the remote-end system or consistent current phases at both ends. These problems present challenges to the applicability of conventional phasor-domain location methods. This paper presents a novel single-ended time domain fault location method for single-phase-to-ground faults, one which fully considers the distributed parameters of the line model. The fitting of transient signals in the time domain is realized to extract the instantaneous amplitude and phase. Then, to eliminate the error caused by assumptions of lumped series resistance in the Bergeron model, an improved numerical derivation is presented for the distributed parameter line model. The instantaneous symmetrical components are extracted for decoupling and inverse transformation of three-phase recording data. Based on the above, the equation of instantaneous phase constraint is established to effectively identify the fault location. The proposed location method reduces the negative effects of fault resistance and the uncertainty of remote end parameters when relying on one-terminal data for localization. Additionally, the proposed fault analysis methods have the ability to adapt to transient processes in power systems. Through comparisons with existing methods in three different systems, the fault position is correctly identified within an error of 1%. Also, the results are not affected by sampling rates, data windows, fault inception angles, and load conditions.**

***Index Terms*—Fault location, distributed parameter line model, transient signal, renewable energy, instantaneous phase.**

Received: June 20, 2023
Accepted: December 10, 2023
Published Online: March 1, 2024
Qiushi Cui (corresponding author) is with the School of Electrical Engineering and with the Liyang Smart City Research Institute, Chongqing University, Chongqing 400044, China (e-mail: qcui@cqu.edu.cn).
DOI: 10.23919/PCMP.2023.000503

## I. Introduction

With the increasing complexity of the power grid, faults in transmission lines can have widespread and significant impacts on the stability and safety of the entire system. According to statistics, single-phase-to-ground faults account for up to 80% of transmission line faults. It is very important to develop new algorithms, models, and techniques that can improve the accuracy and speed of fault location.

Existing transmission line fault location methods are primarily based on the following methods: artificial intelligence, traveling wave, and model-based methods. Artificial intelligence methods [1]–[3] require large amounts of high-quality fault data to generate a good mapping between input measurements and output fault locations. However, the availability of high-quality fault data in practical power systems is limited, often falling short of the required number of fault events needed for effective training [4]. Moreover, intelligent methods are unable to effectively cover various fault scenarios with explainable physical meaning. Traveling-wave-based methods detect the wavefront arrival time of the traveling waves to determine the fault location, using single-ended methods [5], [6] or dual-ended methods [7], [8]. Nevertheless, these methods require extremely high sampling frequency and have difficulty in identifying traveling wave heads. This greatly limits their adaptability and effectiveness.

Model-based methods [9]–[15] construct equations or expressions that relate the line models, available measurements, and fault distance. Because of their clear physical meaning, low sampling rate, and simplicity of the algorithm, model-based methods have been widely applied in practical power systems [16], [17]. Model-based methods can be further classified into single- and dual-ended methods according to data sources. Dual-ended methods use data from both ends and can effectively offset the impact of line parameter variations on the accuracy of fault localization [9], [10]. Nevertheless, these methods require synchronization of measured data and communication channels for the exchange of data between terminals.

Some asynchronous algorithms [18], [19] can be used to calculate or eliminate synchronous angles when dual-ended data are not synchronized. However, in certain situations such as the absence of communication channels or measurement equipment failure at the remote end [20], single-ended methods have distinct advantages. It has advantages of cost-effectiveness, simplicity, and compatibility with existing monitoring systems. It aims to find a solution to reduce the effect of fault resistance and the unknown fault contributed by two-terminal currents. Reference [11] uses negative sequence current to simulate the fault current, while some studies use iterative algorithms to approximate the current after the fault point [12] by assuming that the current phases at both ends of the fault point are consistent. Reference [13] uses multi-source information from two-time sections during both the fault and reclosing time sections. The premise is that the impedance of the opposite-end system remains constant. Reference [14] uses the phasor-domain simplified line model and fast Fourier transform (FFT) to extract the amplitude and phase of the measured voltage and current at a certain frequency. This is based on the assumption of constant fault resistance. In [15], compensated current is used to reduce the negative influence of fault resistance. In summary, these methods [11]–[15] reduce but do not completely eliminate the impact of fault resistance and unknown fault current on fault location.

From the perspective of data types, fault location methods can use either the phasor at fundamental frequency or transient data from instantaneous sampled value measurements. The present single-ended model based methods [11]–[15] are mostly based on fundamental frequency components and phasor-domain models. Some phasor-domain fault location algorithms have been applied in practical systems [1], [12]. However, the growing application of power electronics equipment in power systems has led to challenges related to current limitations and low voltage ride-through. This results in a decrease in system inertia and alterations in steady-state characteristics following a fault occurrence. Thus, it becomes more challenging to extract fundamental frequency components for fault location [22], [23]. In addition, high-speed tripping techniques have difficulty in improving the accuracy of phasor-domain methods. Therefore it is crucial to find a fault analysis method based on transient data in the time domain. To solve the voltage and current distribution in the time domain, existing methods are typically based on the Bergeron model [24]–[26] or on the numerical solutions of the telegrapher's equations. References [9] and [10] use the finite difference and characteristics methods to numerically solve the telegrapher's equation. The Bergeron model assumes a lumped series resistance that can introduce errors, and the accuracy will be affected by the sampling frequency and transmission time [27]. However, current methods of using transient data and time-domain models are based on double-ended data, whereas there is no reported work on fault location based on single-end transient signals.

To overcome the issues of existing single-ended location methods and transient signal analysis, the main contributions of this paper can be summarized as:

1) To effectively extract the instantaneous amplitude and phase in the time domain, the discrete transient data is transformed to time-domain functions by a fitting function model with a Hilbert transform. The fitting function model is a sinusoidal expression. Compared to FFT, the method remains unaffected by the time window and sampling rate.

2) The traditional symmetrical component method based on the frequency domain is not suitable for real-time analysis of fault transient changes. Therefore, based on the proposed sinusoidal expression of the transient data in the time domain, the delay-less extraction of instantaneous symmetrical components and phase shift of the transient signal is obtained.

3) From a micro-circuit model of uniform transmission lines, an improved numerical derivation is developed for the distributed parameter line model based on mathematical induction and limit analysis methods. This derivation eliminates the error caused by assumptions of lumped series resistance in the Bergeron model, and there is no need to consider the influence of transmission time.

4) Based on the above three technical means for analyzing and processing transient signals, the estimation of fault current using single-ended data is achieved. The fault point is identified using the instantaneous initial phase. The location method is not affected by the unknown remote end current, fault resistance, and its time-varying characteristics.

The rest of the paper is organized as follows. Section II and Section III propose three technical means of fault processing for fault location: fitting of the transient signal and its sinusoidal expression, instantaneous symmetrical component transformation, and the line model with full consideration of distributed parameters in the time domain. Section IV elaborates on fault location methods, while Section V validates the above theories and compares the proposed method with other methods. The overall conclusions are given in Section VI.

## II. Formulation of Fitting Functions with Hilbert Transform for Transient Signals

As the proposed method needs to acquire the accurate instantaneous amplitude and initial phase of sampling data, in this section, the discrete sampling data are transformed to time-domain functions by a fitting function model with a Hilbert transform. The constructed fitting function is a sinusoidal expression of transient signals.

### *A. Construction of the Fitting Function Model and Basis Functions*

Reference [28] introduces a sinusoidal expression method for transient signals, but it lacks a comprehensive theoretical analysis for the construction of the function model and basis functions. This paper improves its constructed fitting function, removes redundant terms in the basis functions and demonstrates the feasibility of the approach.

When a fault occurs in a transmission line, the fault current is composed of the fundamental frequency, DC offset attenuation, and attenuation harmonic [29]. Then the fault signal $f(t)$ can be expressed as:

$$f(t)=A_1\cos(\omega_1 t+\varphi_1)+\sum_{k=2}^{q}A_k\mathrm{e}^{-\alpha_k t}\cos(\omega_k t+\varphi_k)+A_{q+1}\mathrm{e}^{-\alpha_{q+1}t} \tag{1}$$

where $A_k$ is the amplitude; $\omega_k$ is the frequency of higher harmonics; $t$ is time; $\varphi_k$ is the initial phase; $q$ is a constant; and $\alpha_k$ ($\alpha_k \geqslant 0$) is the attenuation factor. The above signal can be transformed by trigonometric function transformation and then combined as [30]:

$$f(t)=A_{\mathrm{m}}(t)\sin(\omega t+\varphi(t)) \tag{2}$$

where $A_{\mathrm{m}}(t)$ is the instantaneous amplitude; $\varphi(t)$ is the instantaneous initial phase; $\omega$ is a fixed frequency. By means of trigonometric function transformations, there are:

$$\begin{aligned} f(t)&=A(t)\cos(\omega t)+B(t)\sin(\omega t)\\ A_{\mathrm{m}}(t)&=\sqrt{A^2(t)+B^2(t)}\\ \varphi(t)&=\arctan\left(A(t)/B(t)\right)\end{aligned} \tag{3}$$

where $A(t)$ and $B(t)$ are expressions containing time $t$. It can be seen from the above derivation that as long as $f(t)$ can accurately fit the discrete sampling data, (3) can reflect the corresponding instantaneous amplitude and initial phase characteristics of the original data. Thus, the construction of $A(t)$ and $B(t)$ is important. Continuous functions in function space can be expressed as linear combinations of a series of basis functions, in a similar fashion to the way that each vector in vector space can be expressed as linear combinations of basis vectors. Generally, if a group of bases $\{\phi_i(p)\}_{i=1}^{N}$ are linearly independent, any element in the functional space formed by the bases can be represented by the linear combination of the group of bases [31] $u(p)=\sum_{i=1}^{N}c_i\phi_i(p)$, where $\{c_i\}_{i=1}^{N}$ is a set of undetermined coefficients.

For the construction of the basis function in $A(t)\cos(\omega t)$, to reduce the order of the polynomial in the fitting basis functions and represent the attenuation characteristics of transient signals, $\mathrm{e}^{-st^2}$ is multiplied with polynomial base $\sum_{j=0}^{N}a_j t^j$ to form $A(t)$. Then, $\sum_{j=0}^{N}t^j\mathrm{e}^{-st^2}\cos(\omega t)$ is the same as the bases $\{\phi_i(p)\}_{i=0}^{N}$. By Taylor series expansion of the exponential decay function $\mathrm{e}^{-st^2}$:

$$\mathrm{e}^{-st^2}=\sum_{n=0}^{\infty}\frac{(-st^2)^n}{n!}=1-st^2+\frac{s^2t^4}{2!}-\frac{s^3t^6}{3!}+\cdots \tag{4}$$

We can get that the basic functions of each order in (5) are still linearly independent after they are combined with polynomial operations:

$$A(t)\cos(\omega t)=\sum_{j=0}^{N}a_j t^j\mathrm{e}^{-st^2}\cos(\omega t)=\sum_{j=0}^{N}a_j t^j\left(1-st^2+\frac{s^2t^4}{2!}-\frac{s^3t^6}{3!}+\cdots\right)\cos(\omega t) \tag{5}$$

where $a$ represents the undetermined coefficient; $N$ is the highest degree of the polynomial in $A(t)$; and $s$ represents the set attenuation constant greater than zero.

### *B. Improvement of the Functional Model Using Hilbert Transform*

In order to satisfy the confirmation of $f(t)$ and reduce the number of coefficients of the fitting function, $A(t)$ and $B(t)$ satisfy a certain relationship, i.e., $B(t)$ is the Hilbert transform of $A(t)$. This introduces the orthogonal and energy constraints of time functions $A(t)$ and $B(t)$. For a function $f(t)$, its Hilbert transformation form is written as $h(t)=H[f(t)]$.

Let $A(t)=H[B(t)]$, then $A(t)$ and $B(t)$ satisfy the condition of energy conservation and orthogonality [32]:

$$\begin{cases}\int_{-\infty}^{+\infty}\left[A^2(t)-B^2(t)\right]\mathrm{d}t=0\\ \int_{-\infty}^{+\infty}[A(t)B(t)]\mathrm{d}t=0\end{cases} \tag{6}$$

Compared to the method of setting $A(t)$ and $B(t)$ as independent finite-order polynomials, the constrained sinusoidal expression method can better characterize the overall trend and details of the transient signal. Thus the function model built by the sinusoidal representation method in this paper is given as:

$$f(t)=\left(\sum_{i=0}^{N}a_j t^j\mathrm{e}^{-st^2}\right)\cos(\omega t)+\left(\sum_{j=0}^{N}a_j H\left[t^j\mathrm{e}^{-st^2}\right]\right)\sin(\omega t) \tag{7}$$

The fitting function can have a high degree of expressive power by adjusting the order and attenuation coefficients of the basis function polynomial. Additionally, it can be differentiable infinitely, making it easier to compute its derivatives. Using Leibniz's rule, we can obtain the derivative function of any order. The $n$th order derivative expression of (7) is:

$$f^{(n)}(t)=\sum_{k=0}^{n}\mathrm{C}_n^k\left(\sum_{j=0}^{\infty}a_j t^j \mathrm{e}^{-st^2}\right)^{(n-i)}\omega^i\cos\left(\omega t+\frac{k\pi}{2}\right)+\sum_{k=0}^{n}\mathrm{C}_n^k H\left[\left(\sum_{j=0}^{\infty}a_j t^j \mathrm{e}^{-st^2}\right)^{(n-i)}\right]\omega^i\sin\left(\omega t+\frac{k\pi}{2}\right) \tag{8}$$

The fitting function model, based on the Hilbert transform and the constructed basis functions, ensures accuracy in fitting and the ability to obtain high-order derivatives. In this paper the instantaneous amplitude and initial phase of transient signals can be obtained for the single-end fault location.

In theory, selecting a higher order leads to enhanced fitting accuracy. However, as the order of the fitting function escalates, the number of coefficients to be determined also increases, which in turn increases the computational complexity of obtaining the Hilbert transform of $A(t)$. The specific process of selecting the order is as follows:

1) The fitting order starts at the 5th order and increases incrementally by 5 orders. It stops when the difference in root mean square error (RMSE) between the $N$th and $(N+5)$th order fits is less than 0.01.

2) Starting from the $N$th order, it increases incrementally. The order for fitting is selected as $M$ when the difference in RMSE between the $M$th and $(M+1)$th order fits is less than 0.001.

## III. Derivation of the Voltage and Current Distribution in the Time Domain

In this section, we aim to obtain the accurate distribution of the three-phase voltage and current along transmission lines in the time domain. The stability and minimum error conditions of the existing numerical solutions for the telegrapher's equation have not been mathematically verified [10]. Thus, a new numerical derivation for the distributed parameters line model is presented to accurately solve the voltage and current distribution through the transmission line. This expression does not need to consider the influence of the transmission time of electromagnetic waves on the line. It is used for a single-phase line and requires that the voltage and current are uncoupled. Since the fault recording data is three-phase, decoupling and inverse transformation of transient signals are necessary. Therefore, based on the sinusoidal expression in Section II, the delay-less extraction of instantaneous symmetrical components in the time domain and phase shift of the transient signal is obtained in the following Subsection A.

### *A. Decompose the Transient Signal into Transient Sequence Components*

From Section II, the fault transient signal can be represented by a sinusoidal expression (7) with time-varying amplitude and initial phase at a fixed frequency. The amplitude and initial phase of the three-phase transient signal at a specific time $t$ can be determined. Therefore, the fault signal is endowed with a physical meaning in the phasor domain [33]. The voltage and current at each moment can be expressed as phasors. The phases of transient signals can be shifted and then represented in the phasor domain at each moment. Then each phasor expression can be decomposed using the traditional symmetrical component method. This process can be analogized to the traditional symmetrical component method, as illustrated in Fig. 1. Finally, the sequence components in the time domain can be obtained with their determined amplitude and initial phase. Consequently, the instantaneous sequence components contain the characteristics and physical meaning of the transient signals.

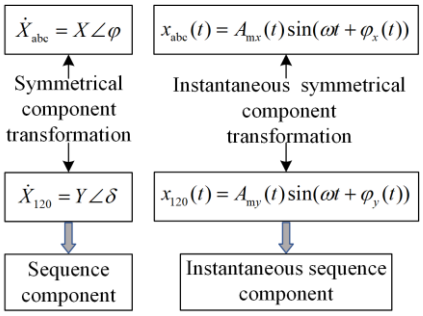


Fig. 1. Symmetrical component transformation and instantaneous symmetrical component transformation.

Based on the above theory, given the transient three-phase current, with A-phase taken as the reference phase, the corresponding instantaneous symmetrical component conversion can be expressed as follows:

$$\begin{cases} i_{a(1)}(t)=\dfrac{1}{3}(I_{am}(t)\sin(\omega t+\varphi_a(t))+I_{bm}(t)\sin(\omega t+\varphi_b(t)+120^\circ)+I_{cm}(t)\sin(\omega t+\varphi_c(t)+240^\circ) \\ i_{a(2)}(t)=\dfrac{1}{3}(I_{am}(t)\sin(\omega t+\varphi_a(t))+I_{bm}(t)\sin(\omega t+\varphi_b(t)+240^\circ)+I_{cm}(t)\sin(\omega t+\varphi_c(t)+120^\circ) \\ i_{a(0)}(t)=\dfrac{1}{3}(I_{am}(t)\sin(\omega t+\varphi_a(t))+I_{bm}(t)\sin(\omega t+\varphi_b(t))+I_{cm}(t)\sin(\omega t+\varphi_c(t)) \end{cases} \tag{9}$$

where $I_{am}(t)$, $I_{bm}(t)$, $I_{cm}(t)$ are the instantaneous amplitudes of three-phase current; $\varphi_a(t)$, $\varphi_b(t)$, and $\varphi_c(t)$ are the instantaneous initial phases of three-phase current; while $i_{a1}(t)$, $i_{a2}(t)$, and $i_{a0}(t)$ represent the instantaneous positive sequence, negative sequence and zero sequence components of the three-phase current $i_a(t)$, respectively. Once the decoupled instantaneous sequence component current has been obtained, the process of inversely transforming it back to the three-phase current follows the same principle as described above. This instantaneous symmetrical component transformation method can be used for the steady-state and

dynamic analysis of various unbalanced operating conditions and asymmetrical faults in power systems.

*B. An improved Numerical Derivation for the Line Model with Distributed Parameters*

Reference [34] introduces a distributed parameter circuit model, based on the micro-circuit model of a uniform transmission line in Fig. 2. However, in its final calculation result, the distributed conductance is ignored in order to simplify the deduction. At the same time, its derivation considers the transmission time of voltage and current waves in the transmission line. However, in practical calculation, the derivation process based on the cascading of micro-circuits already reflects the delay of transmission, so there is no need to reconsider the transmission delay time.

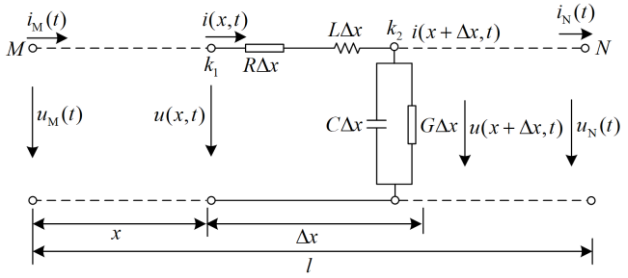


Fig. 2. Detail of a $\Delta x$ section for single-phase transmission line.

Thus, the mathematical induction and limit analysis methods are used to accurately derive the voltage and current distribution along the line. The derivation is detailed in the theory in [34] and fully considers the distributed parameters. From Fig. 2, the current-voltage relationship between the $n$th and $(n-1)$th differential element intervals is given as:

$$\begin{cases} u_n = u_{n-1} - \left( Ri_{n-1} + L\dfrac{\mathrm{d}i_{n-1}}{\mathrm{d}t} \right)\Delta x \\ i_n = i_{n-1} - C\Delta x\dfrac{\mathrm{d}u_n}{\mathrm{d}t} - G\Delta x u_n \end{cases} \tag{10}$$

where $u_n$ and $i_n$ are the voltage and current at the $n$th differential element from the $M$ terminal, respectively, and can be expressed as:

$$\begin{cases} u_n = f_1(u_{\mathrm{M}}, i_{\mathrm{M}}, u'_{\mathrm{M}}, i'_{\mathrm{M}}, u''_{\mathrm{M}}, i''_{\mathrm{M}}, \cdots) \\ i_n = g_1(u_{\mathrm{M}}, i_{\mathrm{M}}, u'_{\mathrm{M}}, i'_{\mathrm{M}}, u''_{\mathrm{M}}, i''_{\mathrm{M}}, \cdots) \end{cases} \tag{11}$$

where $u_{\mathrm{M}}$ and $i_{\mathrm{M}}$ are the voltage and current at the $M$ terminal respectively; and $u'_{\mathrm{M}}$, $i'_{\mathrm{M}}$, $u''_{\mathrm{M}}$, and $i''_{\mathrm{M}}$ are their respective higher-order derivatives.

We can obtain the time-domain expressions of $u_{\mathrm{M}}$ and $i_{\mathrm{M}}$, and their high-order derivatives by the fitting function (7) in Section II. Then, according to (10), the relationship between the current and voltage of the $n$th differential element and the $M$ terminal is given as:

$$\begin{cases} u_n = u_{\mathrm{M}} - \left( Ri_{\mathrm{M}} + L\dfrac{\mathrm{d}i_{\mathrm{M}}}{\mathrm{d}t} \right) n\Delta x + P_n \\ i_n = i_{\mathrm{M}} + Q_n \end{cases} \tag{12}$$

where $P_n$ and $Q_n$ are polynomial functions with respect to $R$, $L$, $C$, $G$, $n$, and $\Delta x^r (r = 1,2,3,\cdots)$.

From (10) and (12), we can derive through recursion as follows:

$$\begin{aligned} Q_n - Q_{n-1} = &\left( -C\frac{\mathrm{d}u_{\mathrm{M}}}{\mathrm{d}t} - Gu_{\mathrm{M}} \right)\Delta x + \left( -GP_n - C\frac{\mathrm{d}P_n}{\mathrm{d}t} \right)\Delta x + \\ &n\left( RC\frac{\mathrm{d}i_{\mathrm{M}}}{\mathrm{d}t} + LC\frac{\mathrm{d}^2 i_{\mathrm{M}}}{\mathrm{d}t^2} + RGi_{\mathrm{M}} + LG\frac{\mathrm{d}i_{\mathrm{M}}}{\mathrm{d}t} \right)\Delta x^2 \end{aligned} \tag{13}$$

$$P_n - P_{n-1} = \left( -RQ_{n-1} - L\frac{\mathrm{d}Q_{n-1}}{\mathrm{d}t} \right)\Delta x \tag{14}$$

Therefore, by using the method of undetermined coefficients and mathematical induction, there are:

$$\begin{cases} u_n(t) = u_{\mathrm{M}}(t) - n\Delta x(Ri_{\mathrm{M}}(t) + Li'_{\mathrm{M}}(t)) + \sum_{j=1}^{\infty} A(j) \\ i_n(t) = i_{\mathrm{M}}(t) - \sum_{j=1}^{\infty} B(j) \end{cases} \tag{15}$$

where

$$\begin{cases} A(j) = \dfrac{\Delta x^{2j}}{(2j)!} \times \prod_{k=-j}^{j-1}(n+k) \sum_{i=0}^{j} C_j^i R^i L^{j-i} (C^j u_{\mathrm{M}}^{(2j-i)}(t) + \\ \quad G^j u_{\mathrm{M}}^{(2j-i-1)}(t)) - \dfrac{\Delta x^{2j+1}}{(2j+1)!} \times \\ \quad \prod_{k=-j}^{j}(n+k) \sum_{i=0}^{j+1} C_{j+1}^i R^i L^{j-i+1} (C^j i_{\mathrm{M}}^{(2j-i+1)}(t) + G^j i_{\mathrm{M}}^{(2j-i)}(t)), \\ B(j) = \dfrac{\Delta x^{2j-1}}{(2j-1)!} \times \prod_{k=1-j}^{j-1}(n+k) \sum_{i=0}^{j} C_{j-1}^i R^i L^{j-i-1} \\ \quad (C^j u_{\mathrm{M}}^{(2j-i-1)}(t) + G^j u_{\mathrm{M}}^{(2j-i-2)}(t)) - \dfrac{\Delta x^{2j}}{(2j)!} \times \\ \quad \prod_{k=1-j}^{j}(n+k) \sum_{i=0}^{i} C_j^i R^i L^{j-i} (C^j i_{\mathrm{M}}^{(2j-i)}(t) + G^j i_{\mathrm{M}}^{(2j-i-1)}(t)) \end{cases} \tag{16}$$

where $n\Delta x = x$ and $x$ represents the distance of a point on the transmission line from the $M$ terminal. When a uniform transmission line is cascaded by an infinite number of lumped parameter circuits, there are $\Delta x \to 0, n \to \infty$. Then,

$$\begin{aligned} \lim_{\substack{n\to\infty \\ \Delta x\to 0}} \Delta x^k \prod_{i=1}^{k}(n+a_i) = &\lim_{\substack{n\to\infty \\ \Delta x\to 0}} \Delta x^k (n^k + p_{k-1}n^{k-1} + \\ &p_{k-2}n^{k-2} + \cdots + p_0) = x^k \end{aligned} \tag{17}$$

Therefore the result is:

$$\begin{cases} A(j)=\dfrac{1}{(2j)!}\displaystyle\sum_{i=0}^{j} l^{2j}C_j^i R^i L^{j-i}(C^j u_{\mathrm{M}}^{(2j-1)}(t)+G^j u_{\mathrm{M}}^{(2j-1-1)}(t))- \\ \qquad \dfrac{1}{(2j+1)!}\displaystyle\sum_{i=0}^{j+1} l^{2j+1}C_{j+1}^i R^i L^{j-i+1}(C^j i_{\mathrm{M}}^{(2j-i+1)}(t)+ \\ \qquad G^j i_{\mathrm{M}}^{(2j-1)}(t)), \\ B(j)=\dfrac{1}{(2j-1)!}\displaystyle\sum_{i=0}^{j-1} l^{2j-1}C_{j-1}^i R^i L^{j-i-1}(C^j u_{\mathrm{M}}^{(2j-i-1)}(t)+ \\ \qquad G^j u_{\mathrm{M}}^{(2j-i-2)}(t))-\dfrac{1}{(2j)!}\displaystyle\sum_{i=0}^{j} l^{2j}C_j^i R^i L^{j-i}(C^j i_{\mathrm{M}}^{(2j-i)}(t)+ \\ \qquad G^j i_{\mathrm{M}}^{(2j-i-1)}(t)) \end{cases} \tag{18}$$

where $l$ represents the length.

To sum up, when the transmission line is in normal operation or in an out-of-zone fault condition, given $u(t)$ and $i(t)$, and their respective derivatives at one terminal ($M$ or $N$), the voltage and current at any other point (including $N$ or $M$ ) can be accurately calculated using the above expression. Compared to the Bergeron model [24]–[26], this model eliminates the model error caused by treating the distributed resistance as lumped resistance. The time-domain expression does not need to consider the influence of transmission time and is theoretically applicable to any length. Compared to the numerical scheme in [10], this expression does not require an optimal choice of time and distance intervals for stability.

## IV. Single-Ended Fault Location Scheme with Short Window Transient Data

The previous two sections provide the sinusoidal expression of transient signals and the distributions of voltage and current along the line in the time domain. In Section II, the short window discrete data are already characterized by the fitting function model in the time domain, whereas in Section III, the distribution of the voltage and current along transmission lines are derived. Then the specific fault points are identified using only single-ended data in this section. Compared to other single-ended location methods, there are no assumptions made on the uncertain remote source impedance and current parameters at both ends. By means of hypothesis testing, equations and criterion functions are constructed to accurately find fault points.

Although the characteristics of different linear time-varying fault resistances are different in the condition of a single-phase-to-ground fault, it is a fact that the phase of the voltage on the fault resistor is identical to the current flowing through the resistance. From Section II, after the frequency $\omega$ of the studied system is determined, the instantaneous initial phases of the voltage and current on the fault resistance remain consistent. Here it assumes that phase A of the line is grounded. As shown in Fig. 3, $M$ and $N$ represent the two ends of the faulty line, $u_R(t)$ and $i_{\mathrm{M}}(t)$ represent the phase A voltage and current calculated from the $M$ terminal to the fault location. Similarly, $i_{\mathrm{N}}(t)$ represents the phase A current flowing into the fault resistance from the $N$ terminal.

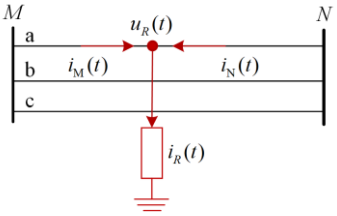


Fig. 3. Diagram of single-phase to ground short circuit.

$u_R(t)$ and $i_R(t)$ on the fault resistor can be expressed as follows:

$$\begin{aligned} u_R(t)&=U_R(t)\sin(\omega t+\varphi_{u_R}(t))= \\ &\quad A_{u_R}(t)\cos(\omega t)+B_{u_R}(t)\sin(\omega t) \\ i_R(t)&=i_{\mathrm{M}}(t)+i_{\mathrm{N}}(t)=I_R(t)\sin(\omega t+\varphi_{i_R}(t))= \\ &\quad A_{i_{\mathrm{M}}}(t)\cos(\omega t)+B_{i_{\mathrm{M}}}(t)\sin(\omega t)+ \\ &\quad A_{i_{\mathrm{N}}}(t)\cos(\omega t)+B_{i_{\mathrm{N}}}(t)\sin(\omega t) \end{aligned} \tag{19}$$

where $U_R(t)$ is the instantaneous amplitude of $u_R(t)$; $I_R(t)$ is the instantaneous amplitude of $i_R(t)$; $A_{u_R}$, $B_{u_R}$, $A_{i_{\mathrm{M}}}(t)$, $B_{i_{\mathrm{M}}}(t)$, $A_{i_{\mathrm{N}}}(t)$ and $B_{i_{\mathrm{N}}}(t)$ are expressions about time $t$ in the fitting function; $\varphi_{uR}(t)$ and $\varphi_{iR}(t)$ are the instantaneous initial phases, and can be transformed into:

$$\begin{cases} \varphi_{u_R}(t)=\arctan(A_{u_R}(t)/B_{u_R}(t)) \\ \varphi_{i_R}(t)=\arctan(A_{i_{\mathrm{M}}}(t)+A_{i_{\mathrm{N}}}(t))/(B_{i_{\mathrm{M}}}(t)+B_{i_{\mathrm{N}}}(t)) \end{cases} \tag{20}$$

Based on the consistency of the instantaneous initial phase, there are:

$$\frac{A_{i_{\mathrm{M}}}(t)+A_{i_{\mathrm{N}}}(t)}{B_{i_{\mathrm{M}}}(t)+B_{i_{\mathrm{N}}}(t)}=\frac{A_{u_R}(t)}{B_{u_R}(t)} \tag{21}$$

We assume that the voltage and current from one terminal at any point $S_j$ is $u_{S_j}$ and $i_{M_{S_j}}$. By employing the fitting function model in Section II and the time-domain expression of the voltage and current distribution in Section III, $A_{uS_j}(t)$, $B_{uS_j}(t)$, $A_{i_{\mathrm{M}}S_j}(t)$, and $B_{i_{\mathrm{M}}S_j}(t)$ at any point along the line can be obtained, while $A_{i_{\mathrm{N}}S_j}(t)$ and $B_{i_{\mathrm{N}}S_j}(t)$ are unknown. It is not possible to directly use the instantaneous phases of the current and voltage at one end of the circuit for fault localization.

From the constructed fitting function in Section II, there is:

$$i_{Ns_j}=\left(\sum_{j=0}^{N}a_j t^j \mathrm{e}^{-st^2}\right)\cos(\omega t)+\left(\sum_{j=0}^{N}a_j H\left[t^j \mathrm{e}^{-st^2}\right]\right)\sin(\omega t) \tag{22}$$

where

$$\begin{cases} A_{i_N S_j}(t) = \sum_{j=0}^{N} a_j t^j \mathrm{e}^{-st^2} \\ B_{i_N S_j}(t) = H(A_{i_N}(t)) = \sum_{j=0}^{N} a_j H\left[t^j \mathrm{e}^{-st^2}\right] \end{cases} \tag{23}$$

However, the coefficient $\{a_j\}_{j=0}^{N}$ is unknown. Based on the logic of hypothesis testing, the fault location can be searched from the $M$ terminal to the $N$ terminal. Assuming that $S_j$ is the fault point, then according to (21):

$$\sum_{j=0}^{N} a_j \left[A_{uS_j}(t) t^j \mathrm{e}^{-st^2} - B_{uS_j}(t) H(t^j \mathrm{e}^{-st^2})\right] = A_{i_M S_j}(t) B_{uS_j}(t) - B_{i_M S_j}(t) A_{uS_j}(t) \quad (t = 0 - \frac{1}{2} t_d) \tag{24}$$

We use part of the sampling time $0 - \frac{1}{2}t_d$, with the time interval $\Delta t$, and substitute it into (24) to solve for the hypothetical coefficient $\{a_j\}_{j=0}^{N}$. Thus the virtual coefficient $\{a_j\}_{j=0}^{N}$ of $A_{i_N S_j}(t)$ and $B_{i_N S_j}(t)$ at every point along the line can be obtained. To determine whether the point $S_j$ is the fault point, the other half of the sampling time $\frac{1}{2}t_d - t_d$ is used to verify the consistency of instantaneous initial phases. The sampling time $\frac{1}{2}t_d - t_d$ with the time interval $\Delta t$ is brought into the criterion function as follows to verify the fault point:

$$f(S_j) = | A_{us_j}(t')(B_{i_M S_j}(t') + B_{i_N S_j}(t')) - B_{us_j}(t')(A_{i_M S_j}(t') + A_{i_N S_j}(t'))|, \quad t' = \frac{1}{2}t_d - t_d \tag{25}$$

The fault location is one where (25) is zero. However, in practical application, considering the influence of various errors and calculation accuracy, it considers that the point $S_j$ in the search interval that minimizes the value of (25) is the fault point $S_f$. Therefore there is:

$$f(S_j) = \min(f(S_j)) \quad (j = 1, 2, 3, \cdots) \tag{26}$$

To decrease the computational complexity, two iterations [10] are used for the distance step of the search in Fig. 4. In the initial iteration, the approximate location $S_{f'}$ is determined within the entire transmission line $[0, l]$, by using a relatively wide distance step size $\Delta x_1$. In the second iteration, it uses an exhaustive search and sweep through the interval $[S_{f'} - \Delta x_1, S_{f'} + \Delta x]$ with a small step size $\Delta x_2$ to find the precise position $S_f$.

Figure 5 illustrates the research ideas and process of the fault location algorithm encompassing Sections II, III, and IV. In Section II, fitting of transient signals is performed in the time domain to extract the instantaneous amplitude and phase. In Section III, a numerical derivation based on mathematical induction and limit analysis methods is proposed to accurately determine the voltage and current distribution through the transmission line. Based on the above, in Section IV, an equation of instantaneous phase constraint and criterion function is established to effectively identify the fault location.

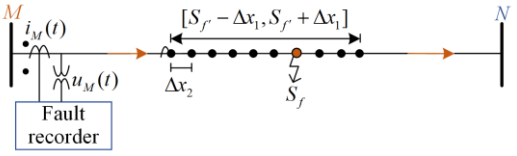


Fig. 4. Details of the fault location algorithm.

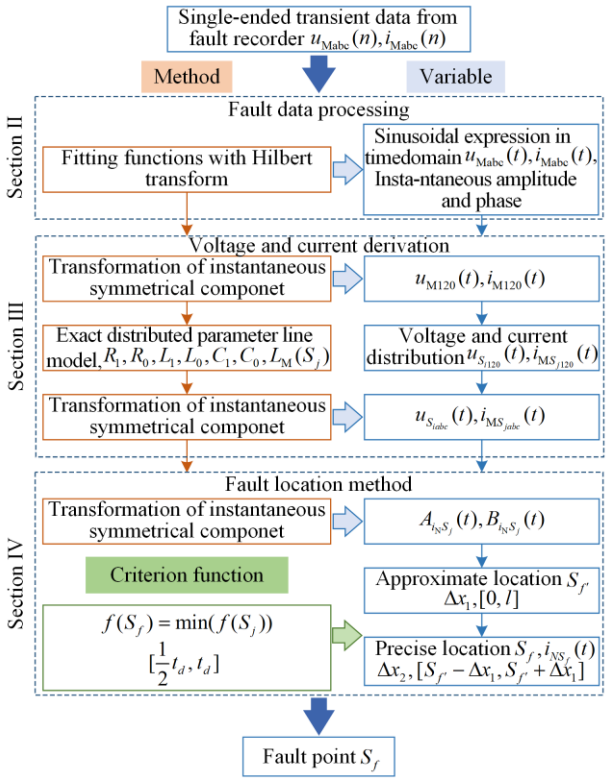


Fig. 5. Flowchart of the proposed fault location algorithm.

## V. Case Studies

To verify the effectiveness and correctness of the proposed method, we use fault data from a simulated system implemented on the MATLAB/Simulink platform and a regional power grid in China. The proposed theories in Sections II, III and IV are tested and validated in the following subsections.

### *A. Validation of Transient Signal Fitting Function*

To verify the effectiveness of the proposed method in Section II, the transient signal fitting function on the simulated signal is analyzed. Based on the MATLAB/Simulink platform, the simulation model of the DFIG grid-connected operation shown in Fig. 6 is established, including the model of the AC/DC/AC converter of the doubly-fed wind power generation system. The grid side of the AC/DC/AC converter adopts the

stator voltage-oriented control strategy, and the rotor side adopts the stator flux-oriented control strategy.

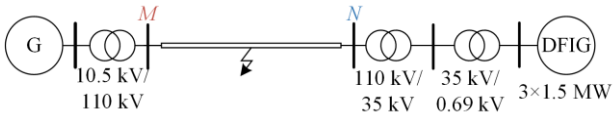


Fig. 6. Two-terminal transmission system with wind turbines at *N* terminal.

There are 3 wind turbines, the rated voltage of each is 690 V, and the rated capacity is 1.5 MW. The turbines are connected to the power grid through step-up transformers (0.69/35 kV) and a main transformer (35/110 kV). The transmission line length is 100 km, and the line parameters (positive sequence and zero sequence) are: $R_1 = 0.1273\ \Omega$/km , $L_1 = 0.9337$ mH/km , $C_1 = 0.0141\ \mu$F/km, $R_0 = 0.3864\ \Omega$/km, $L_0 = 4.1264$ mH/km, and $C_0 = 0.0081\ \mu$F/km . Assuming that the breaker trips at 20 ms, the voltage and current sampling data at the *M* and *N* terminals are fitted in the different cases listed in Table I. In these scenarios, different types of fault resistance and fault distance values are considered. The sampling rate is 2000 Hz, and the sampling time is 20 ms.

TABLE I
SETTING OF FAULT PARAMETERS

| Case | Phase angle Difference (°) | Fault resistance | Fault Distance (km) |
|---|---|---|---|
| 1 | 30 | $R(t) = 0.1$ | 5 |
| 2 | 30 | $R(t) = 0.1 + 10t$ | 15 |
| 3 | 60 | $R(t) = 0.1 + 10t^2$ | 25 |
| 4 | 90 | $R(t) = 10 + 10^{30t}$ | 30 |

Figure 7 shows the fitting curves and fault signals of phase A voltage. It can be seen that the integration of renewable energy into the grid introduces nonlinear loads, which generate harmonics, resulting in the presence of additional harmonic components in the fault waveform. The *RMSE* is calculated after normalizing the data in Table II using $x' = \dfrac{x - \min(x)}{\max(x) - \min(x)}$. The *RMSE* at each terminal is calculated as: $RMSE = \sqrt{\dfrac{1}{N}\sum_{i=1}^{n}\left(Y_i' - f'(x_i)\right)^2}$, where $Y_i'$ and $f'(x_i)$ are the normalized sampling and fitting data, respectively. It can be seen that the proposed fitting method in Section 2 performs well when dealing with fault transient signals. The theoretical derivation and the simulation demonstrate that the sinusoidal expression of the fitting function with the Hilbert transform can ensure fitting accuracy.

TABLE II
FITTING ERROR IN DIFFERENT FAULT CONDITIONS

| Case | RMSE of three phases | | | |
|---|---|---|---|---|
| | $U_M$ | $I_M$ | $U_N$ | $I_N$ |
| 1 | 0.2743 | 0.0158 | 0.4848 | 0.0261 |
| 2 | 0.0802 | 0.033 | 0.1209 | 0.0097 |
| 3 | 0.0684 | 0.0433 | 0.018 | 0.0338 |
| 4 | 0.0395 | 0.0461 | 0.0308 | 0.05 |

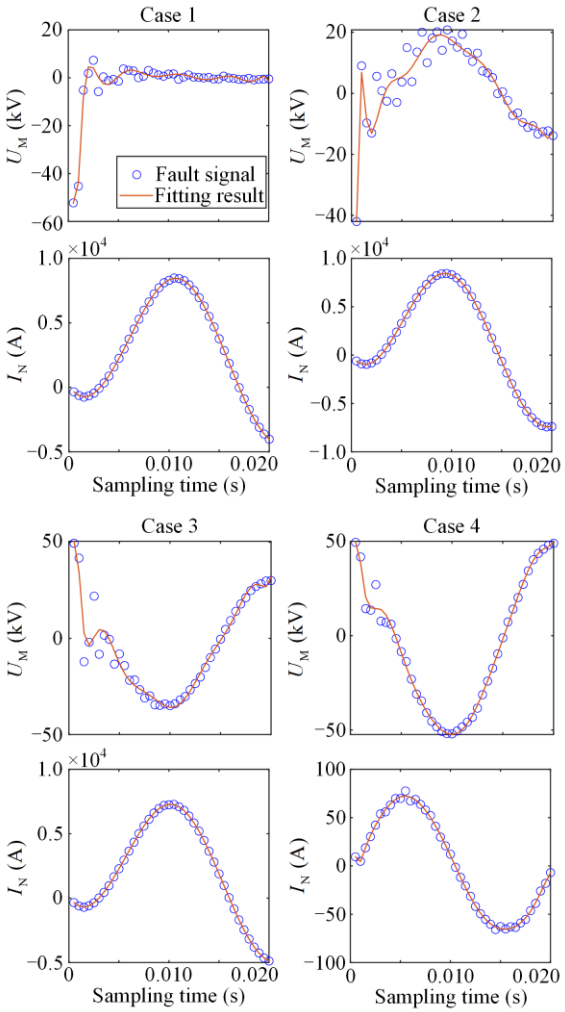


Fig. 7. The performance of the fitting functions using phase A voltage and current at the *M* terminal in different cases.

To verify the accuracy of the fitting function at different sampling rates, different sampling frequencies of 1200 Hz, 1600 Hz, 2400 Hz and 4000 Hz are tested. The simulation data is a set of fault current, and the fitting results are shown in Fig. 8. It can be seen that the proposed fitting method performs well when dealing with fault transient signals with different sampling rates.

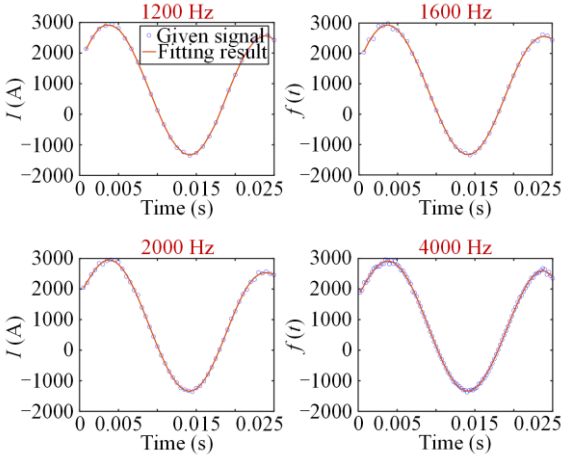


Fig. 8. The fitting results at different sampling rates.

### *B. Validation of the Derivation of the Voltage and Current Distribution Through the Transmission Line*

For the deduced line model in Section III, when $j$ approaches infinity, the calculated $u_{\mathrm{N}}(t)$ and $i_{\mathrm{N}}(t)$, and the sampled value (real value) of $N$-terminal are equal. However, it is unrealistic to take $j$ to infinity, and therefore errors will inevitably occur. The effect of the value $j$ on the accuracy is further studied to verify the correctness in steady-state, and the accuracy of the transient calculation is compared with the Bergeron model.

*1) Validation at Normal Steady States*

To verify the correctness of the derived model in the case of a single-phase steady state, the 1000 kV single-phase and single-source power transmission system is taken as an example.

The length of the line is 500 km, the internal impedance of the power source is $Z_{\mathrm{G}} = 21.5 + \mathrm{j}122.6\,\Omega$, the load impedance is $Z_{\mathrm{L}} = 1500\,\Omega$, and the line parameters are: $R = 0.013\,33\,\Omega/\mathrm{km}$, $L = 0.8473\,\mathrm{mH/km}$, and $C = 0.0139\,\mu\mathrm{F/km}$. We sample 10 points in each cycle, and take 5 points to compare the sampled value with the calculated value. In Table III, $i_{\mathrm{M_s}}$ and $i_{\mathrm{N_s}}$ are the sampling values of the current at both ends of $M$ and $N$, respectively. $i_{\mathrm{N_c}}$ is the calculated value of the current at the $N$ terminal, and the absolute error is $\mathrm{d}i_{\mathrm{N}} = \left|i_{\mathrm{Nc}} - i_{\mathrm{Ns}}\right|$. From (16), the relationship between the order $r$ of $\Delta x$ and $j$ is $r = 2j - 1$. As shown in Table III, as the value of $j$ for $\Delta x$ increases, the absolute error between the calculated value and the sampled value decreases. When $\Delta x$ is taken to be the 7th order, the maximum absolute error is already less than 2 A, and the sampled and calculated values are basically the same.

TABLE III
COMPARISON OF N-TERMINAL MEASURED CURRENT AND CALCULATED CURRENT

| Current (A) | | Sampling value, calculated value, absolute error | | | | |
|---|---|---|---|---|---|---|
| | | 1 | 2 | 3 | 4 | 5 |
| $i_{\mathrm{Ns}}$ | Sampled value | 726.8 | 765.8 | 729.8 | 622.4 | 454.0 |
| $i_{\mathrm{Ms}}$ | Sampled value | 1373.6 | 669 | −101.0 | −861.2 | −1537.1 |
| $i_{\mathrm{Nc}}$ | $\Delta x^{1}$ | 1373.6 | 669.0 | −101.0 | −861.2 | −1537.1 |
| | $\Delta x^{3}$ | 696.0 | 769.6 | 767.9 | 691.0 | 546.5 |
| | $\Delta x^{7}$ | 728.6 | 767.6 | 731.5 | 623.8 | 455.0 |
| | $\Delta x^{13}$ | 728.6 | 767.6 | 731.5 | 623.8 | 455.0 |
| | $\Delta x^{19}$ | 728.6 | 767.6 | 731.5 | 623.8 | 455.0 |
| $\mathrm{d}i_{\mathrm{N}}$ | $\Delta x^{1}$ | 646.7 | 96.8 | 830.9 | 1483.6 | 1991.2 |
| | $\Delta x^{3}$ | 30.8 | 3.8 | 38.0 | 68.6 | 92.4 |
| | $\Delta x^{7}$ | 1.7 | 1.7 | 1.6 | 1.4 | 1 |
| | $\Delta x^{13}$ | 1.7 | 1.7 | 1.6 | 1.4 | 1 |
| | $\Delta x^{19}$ | 1.7 | 1.7 | 1.6 | 1.4 | 1 |

*2) Comparison with the Bergeron Model*

The accuracy of this proposed model and the Bergeron model cannot be compared through the simulation platform. Therefore, we use the actual fault information of three different out-of-area faults of a power grid in China to achieve a comparative analysis. The line length is 92.559 km, and the line parameters (zero sequence) are: $R_0 = 0.2013\,\Omega/\mathrm{km}$, $L_0 = 2.5035\,\mathrm{mH/km}$, and $C_0 = 0.0081\,\mu\mathrm{F/km}$, and the sampling frequency is 1200 Hz. The instantaneous component transformation proposed in Section III is used to obtain the zero sequence component. From the comparative results shown in Fig. 9, although the current values calculated by the proposed model and the Bergeron model are largely equal, the voltage values calculated by this model are closer to the true values than those calculated by the Bergeron model. In addition, the absolute squared errors are shown in Table IV to quantify the difference between the calculated values and sampled values.

TABLE IV
ABSOLUTE SQUARED ERRORS OF THE PROPOSED MODEL AND THE BERGERON MODEL

| $\sqrt{\mathrm{SSE}}$ | Model | Case1 | Case2 | Case3 |
|---|---|---|---|---|
| Voltage | Bergeron | $2.21\times10^{4}$ | $1.40\times10^{4}$ | $3.11\times10^{4}$ |
| | Proposed | $1.90\times10^{4}$ | $1.14\times10^{4}$ | $2.40\times10^{4}$ |
| Currrent | Bergeron | $0.92\times10^{4}$ | $1.55\times10^{4}$ | $1.13\times10^{4}$ |
| | Proposed | $0.8\times10^{4}$ | $1.33\times10^{4}$ | $1.1\times10^{4}$ |

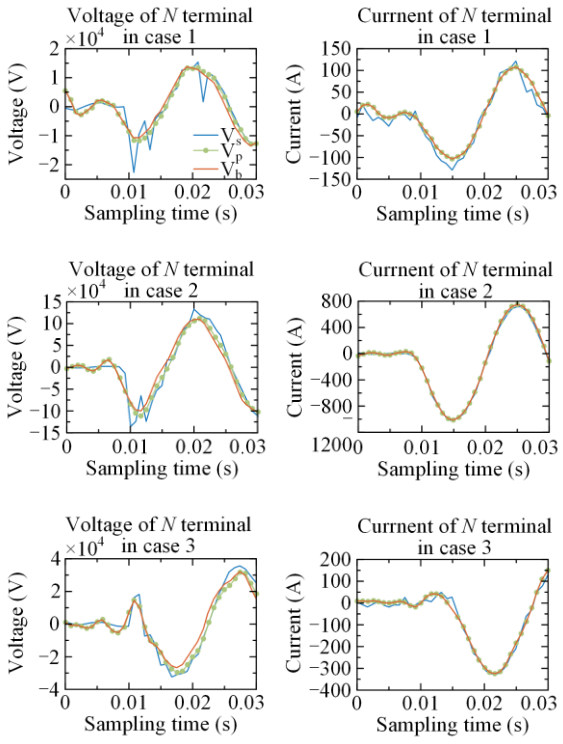


Fig. 9. Comparative result between the proposed model and the Bergeron model.

### *C. Validation of the Fault Location Scheme*

#### *1) Validation of Different Transmission Systems and Practical Cases*

Three transmission systems are tested with different parameters to verify the proposed fault location method: 1) the traditional dual-power transmission line without access to renewable energy; 2) the dual-power transmission line with wind farms connected to the grid; and 3) the single-power transmission line. A simulation system model of 110 kV is developed as shown in Fig. 6, using the power supply and line parameters included in Subsection A of Section V. The phase angle difference between the two equivalent sources is 30°.

In addition, two practical cases from a regional power grid in China that occurred in 2019 are selected for verification. The data includes A-phase-to-ground and B-phase-to-ground faults, with a sampling frequency of 1200 Hz. For fault location, 36 data points are selected following the fault, and the corresponding time window is from 0.000 83 s to 0.03 s. The line conductance is neglected in this analysis.

To verify the effectiveness of the fault location method and its adaptability to different fault resistances, four types of fault resistance are shown in Table V. There are three different line lengths with different iterative search step sizes as shown in Table VI. The fault recorder is installed at the *M* terminal. The fault occurrence time is 0.015 s, with a data sampling rate of 2000 Hz, and a sampling time window of 0.015 s to 0.045 s. Taking phase-A-to-ground fault as an example, the fault settings and absolute fault location errors are shown in Table VI.

TABLE V
FAULT RESISTANCE IN SIMULATION

| Fault resistance | Fault resistance expression | Time interval (s) | Corresponding value range |
|---|---|---|---|
| $R_1(t)$ | $400t$ | 0.015–0.045 | 6–18 |
| $R_2(t)$ | $10+10^{40t}$ | 0.01–0.045 | 13.98–73 |
| $R_3(t)$ | $80-8^{20t}$ | 0.015–0.045 | 78.1–73.5 |
| $R_4(t)$ | 100 | 0.015–0.045 | 100 |

TABLE VI
FAULT LOCATING RESULTS OF ALL CASES

| Case | Fault distance (km) | Fault resistance ( Ω ) | Fuzzy interval | $S_f$ (km) | Error (%) |
|---|---|---|---|---|---|
| System1 | 20 | $R_1$ | [18, 22] | 20.1 | 0.10 |
| $l=100$ km | 45.5 | $R_1$ | [44, 48] | 45.3 | 0.20 |
| $\Delta x_1=2$ km | 60.25 | $R_2$ | [60, 64] | 60.3 | 0.05 |
| $\Delta x_2=0.1$ km | 80 | $R_3$ | [78, 82] | 80.1 | 0.10 |
| System2 | 10 | $R_3$ | [9, 11] | 10.00 | 0.00 |
| $l=50$ km | 25.2 | $R_1$, $R_2$ | [24, 26] | 25.05 | 0.30 |
| $\Delta x_1=1$ km | 35.6 | $R_4$ | [35, 37] | 35.65 | 0.10 |
| $\Delta x_2=0.05$ km | 40.1 | $R_3$, $R_4$ | [40, 42] | 40.20 | 0.16 |
| System3 | 5.32 | $R_3$ | [4, 6] | 5.400 | 0.32 |
| $l=25$ km | 15.36 | $R_2$, $R_3$, $R_4$ | [14, 16] | 14.975 | 0.14 |
| $\Delta x_1=1$ km | 20.84 | $R_1$, $R_2$, $R_3$, $R_4$ | [20, 22] | 20.825 | 0.06 |
| $\Delta x_2=0.025$ km | 10.7 | $R_4$ | [10, 12] | 10.665 | 0.14 |
| Practical case | 40.12 | | [39, 41] | 40.05 | 0.051 |
| $l=134.65$ km | 100.875 | | [100, 102] | 100.85 | 0.018 |

Because of space constraints, only the location result diagram of the system (1) is provided. At each detection point, the value of the criterion function in (26) is shown in Fig. 10. It can be seen that the lowest point of the criterion function curve is the calculated fault point. In all location results, the maximum relative errors do not exceed 1% , as shown in Table VI. The minimum value of the criterion function at the fault point is not strictly zero. Thus the instantaneous initial phases of the voltage and current on the fault resistance are not strictly equal, but are consistent. From the above validation of simulated cases and practical cases, it can be concluded that different factors such as transmission systems, fault positions, fault resistance values, and time-varying characteristics do not affect the accuracy and effectiveness of the fault location method. Also, this method

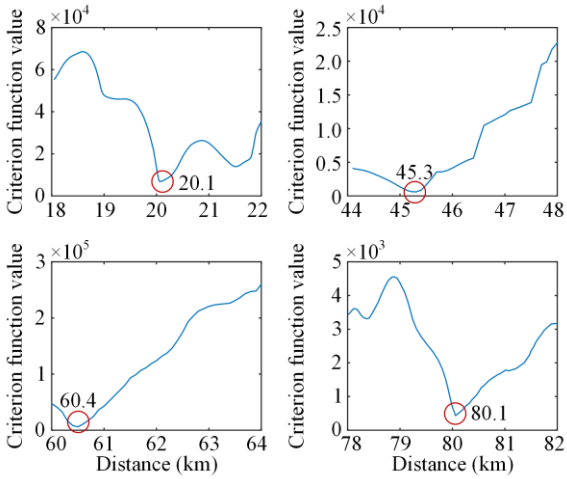


Fig. 10. Fault location results in the system (1).

can use a limited amount of existing fault waveform data for localization. It is applicable to practical fault scenarios.

*2) Comparison with the Existing Fault Location Method*

The fault location method is further validated by comparing it with the existing single-ended location method in [14], which is based on the simplified phasor based line model and uses FFT to extract the amplitude and phase of the measured voltage and current at the fundamental frequency. Based on the assumption of constant fault resistance, the line reactance is calculated to locate the fault. Since the existing methods based on transient data and time-domain distribution parameter line models all use dual-ended data, they are not considered for comparison.

The system (2) which is a dual-power transmission line with wind farms connected to the grid is tested with four types of time-varying resistances in Table V. Using the power supply and line parameters included in Subsection A of Section V, the fault locations are through the entire length of the transmission line (16 fault locations, 300 km, $\Delta x_1 = 1$ km, $\Delta x_2 = 0.005$ km). The fault location results are shown in Fig. 11. It can be concluded that the proposed method presents higher fault location accuracy than the existing method based on the steady-state data and simplified line model. This is due to the fact that the FFT used in [14] for extracting the amplitude and phase at a certain frequency is not unique by periodic extension. Additionally, the method assumes that the current phases at both ends are consistent, so the location method is not suitable for time-varying resistance.

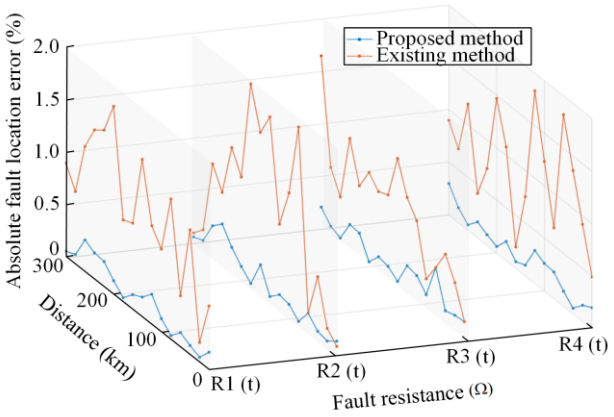


Fig. 11. Absolute fault location errors with different location methods.

*3) The Effects of Different Factors on the Fault Location Accuracy*

To assess the effect of different factors on the fault location accuracy, tests are conducted at various sampling rates, data windows, fault inception angles, and load conditions under system (2). The power supply and line parameters are the same as those in Subsection A of Section V. Figure 12 shows the average fault location errors of the resistance $R_1(t)$ of the phase-A-to-ground faults with different factors.

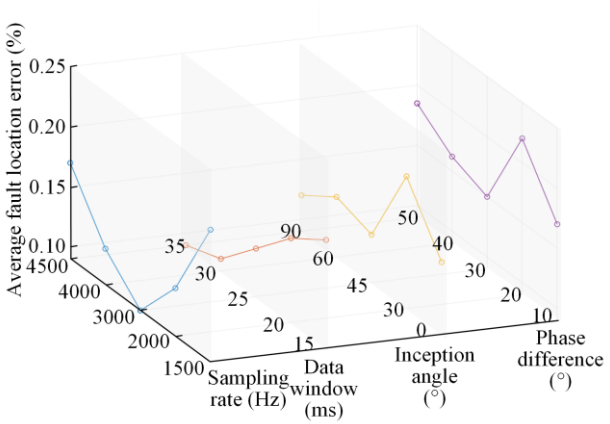


Fig. 12. Average fault location errors with different factors.

At the same time, errors caused by line parameters and measurement noise should be considered. Referring to [35], [36], Gaussian noise with different signal-to-noise ratios (SNR) is introduced to test the proposed method. Noise levels at 20 dB, 30 dB, 40 dB, and 50 dB are added to the voltage and current signals acquired from MATLAB/Simulink. Also, referring to [10], [37], 0.5%, 1%, 1.5% and 2% parameter errors are added to the parameter matrices of the transmission line, respectively. This adjustment is only for the fault location algorithm, while the example test system in Simulink remains unchanged.

From the results shown in Fig. 12, it can be seen that excessively high sampling rates do not significantly improve the fault localization accuracy of the proposed method. This is because excessively high sampling rates can cause overfitting of the curve and increase the calculation error of voltage and current along the line. Meanwhile, the accuracy decreases with the extension of the sampling time window, because a longer sampling time contains more abundant fault information. The fault position can be correctly identified within an error of 1%, and the results are not affected by fault inception angles and load conditions. Also, from the results shown in Table VII, the proposed method shows acceptable accuracy within 1% with different error settings. It also shows that the proposed fault location algorithm has a certain robustness. It can be concluded that noise level and line parameter error are not the dominant factors affecting fault location accuracy. In fact, the location accuracy is mainly affected by the fitting function, the accuracy of the distribution parameter line model, fault criteria function, etc.

Table VII
LOCATION ERRORS UNDER DIFFERENT NOISE LEVELS AND PARAMETER ERRORS

| Factor | Value | Maximum absolute errors (%) | Average absolute errors (%) |
|---|---|---|---|
| Noise level | 20dB | 0.52 | 0.27 |
| | 30dB | 0.44 | 0.21 |
| | 40dB | 0.68 | 0.39 |
| | 50dB | 0.45 | 0.25 |
| Parameter error | 0.50% | 0.61 | 0.33 |
| | 1% | 0.55 | 0.24 |
| | 1.50% | 0.64 | 0.35 |
| | 2% | 0.75 | 0.42 |

## VI. CONCLUSION

This paper proposes a novel single-ended time-domain fault location method for power systems with high-speed tripping techniques and extensive application of power electronics equipment. Unlike existing methods, the proposed approach uses fault transient data from a single terminal, thus eliminating the need for assumptions on uncertain remote source impedance and current parameters at both ends. Accurate fitting of discrete fault transient signals is achieved. The constructed fitting function model enables the extraction of crucial information such as instantaneous amplitude, instantaneous initial phase, and higher-order derivatives. This methodology allows effective analysis and assessment of the transient characteristics of power systems. Then, a numerical derivation based on mathematical induction and limit analysis methods is proposed to accurately determine the voltage and current distribution through the transmission line. The fault location method proposed in this study exhibits superior accuracy compared to the model-based method relying on the existing Bergeron model. Extensive simulations have been conducted to validate the proposed theories, demonstrating their robust performance. The fault location results show that the fault position can be correctly identified within an error of 1%. The method offers several notable advantages, including clear physical interpretation, simplified calculations, and strong practical applicability. It requires a short data window, operates with low sampling rate requirements, and exhibits a certain degree of noise resistance.

## ACKNOWLEDGMENT

Not applicable.

## AUTHORS' CONTRIBUTIONS

Jian Luo: conceptualization and methodology. Yao Liu: conceptualization, methodology, validation, formal analysis, writing original draft, reviewing and editing. Qiushi Cui: conceptualization, validation, reviewing and editing. Jiayong Zhong: formal analysis, supervision, reviewing and editing. Lin Zhang: formal analysis and supervision. All the authors read and approved the final manuscript.

## FUNDING

This work is carried out without the support of any funding agency.

## AVAILABILITY OF DATA AND MATERIALS

Please contact the corresponding author for data material request.

## DECLARATIONS

Competing interests: The authors declare that they have no known competing financial interests or personal relationships that could have appeared to influence the work reported in this article.

## AUTHORS' INFORMATION

**Jian Luo** received the D.R. degree from Chongqing University, Chongqing, China. He is currently a professor with the School of Electrical Engineering, Chongqing University. His research interest is in the research and application of power system protection and control.

**Yao Liu** received the B.E. degree in electrical engineering from Taiyuan University of Technology, Taiyuan, China. She is currently pursuing the M.S. degree in electrical engineering with Chongqing University, Chongqing, China. Her research interest is in the research and application of power system protection and control.

**Qiushi Cui** received the M.Sc. degree from the Illinois Institute of Technology, and the Ph.D. degree in electric engineering from McGill University. He is currently an associate professor with the School of Electrical Engineering and with the Liyang Smart City Research Institute, Chongqing University, Chongqing, China. He was working as a postdoctoral researcher with Arizona State University (ASU) and served as the associate director of Machine Learning Laboratory for Power Systems, Ira A. Fulton Schools of Engineering, ASU. His research interests are in the areas of machine learning and big data applications in power systems, power system protection, smart cities, microgrid, EV integration, and real-time simulation in power engineering.

**Jiayong Zhong** received the D.R. degree in Electrical Engineering from chongqing University , Chongqing, China. He works in State Grid Chongqing Electric Power Company Research Institute, Chongqing, China. His work centers on Digitalization of power system.

**Lin Zhang** works in State Grid Chongqing Electric Power Company Research Institute, Chongqing, China. His research interests include power system stability and control, and optimized operation of new energy systems.

## REFERENCES


[1] S. Das, S. Santoso, and A. Gaikwad *et al*., "Impedance-based fault location in transmission networks: theory and application," *IEEE Access*, vol. 2, pp. 537-557, May 2014.

[2] Z. Wang, Z. Chen and M. Paolone, "A data-driven fault location algorithm based on the electromagnetic time reversal in mismatched media," *IEEE Transactions on Power Delivery*, vol. 37, no. 5, pp. 3709-3721, Oct. 2022.

[3] Y. Wang, T. Wang and L. Liu, "A fault segment location method for distribution networks based on spiking neural P systems and Bayesian estimation," *Protection and Control of Modern Power Systems*, vol. 8, no. 3, pp. 1-12, Jul. 2023.

[4] L. Song, Y. Li, and N. Lu, "Profilesr-gan: a gan based super-resolution method for generating high-resolution load profiles," *IEEE Transactions on Smart Grid*, vol. 13, no. 4, pp. 3278-3289, Jul. 2022.

[5] H. Shu, S. Wang and S. Lei, "Single-ended protection method for hybrid HVDC transmission line based on transient voltage characteristic frequency band," *Protection and Control of Modern Power Systems*, vol. 8, no. 2, pp. 1-11, Apr. 2023.

[6] H. Shu, X. Liu, and X. Tian, "Single-ended fault location for hybrid feeders based on characteristic distribution of traveling wave along a line," *IEEE Transactions on Power Delivery*, vol. 36, no. 1, pp. 339-350, Feb. 2021.

[7] L. Cheng, T. Wang, and Y. Wang, "A novel fault location method for distribution networks with distributed generations based on the time matrix of traveling-waves," *Protection and Control of Modern Power Systems*, vol. 7, no. 1, pp. 1-11, Oct. 2022.

[8] Z. Qi, Z. Huang and Y. Chen, "Impedance fault location technology for a distribution network based on a zero-sequence component," *Power System Protection and Control*, vol. 51, no.6, pp. 54-62, May 2023. (in Chinese)

[9] A. Gopalakrishnan, M. Kezunovic, and S. McKenna *et al*., "Fault location using the distributed parameter transmission line model," *IEEE Transactions on Power Delivery*, vol. 15, no. 4, pp. 1169-1174, Oct. 2000.

[10] D. Lu, Y. Liu, and Q. Liao *et al*., "Time-domain transmission line fault location method with full consideration of distributed parameters and line asymmetry," *IEEE Transactions on Power Delivery*, vol. 35, no. 6, pp. 2651-2662, Dec. 2020.

[11] M. Choi, S. Lee, and D. Lee *et al*., "A new fault location algorithm using direct circuit analysis for distribution systems," *IEEE Transactions on Power Delivery*, vol. 19, no. 1, pp. 35-41, Jan. 2004.

[12] S. Lee, M. Choi, and S. Kang *et al*., "An intelligent and efficient fault location and diagnosis scheme for radial distribution systems," *IEEE Transactions on Power Delivery*, vol. 19, no. 2, pp. 524-532, Apr. 2004.

[13] L. Ji, X. Tao, and Y. Fu *et al*., "A new single ended fault location method for transmission line based on positive sequence superimposed network during auto-reclosing," *IEEE Transactions on Power Delivery*, vol. 34, no. 3, pp. 1019-1029, Jun. 2019.

[14] K. Jia, D. Thomas, and M. Sumner, "A new single-ended fault-location scheme for utilization in an integrated power system," *IEEE Transactions on Power Delivery*, vol. 28, no. 1, pp. 38-46, Jan. 2013.

[15] R. ˇZivanovi´c, "Evaluation of transmission line fault-locating techniques using variance-based sensitivity measures," in *16th Power Systems Computation Conference*, Glasgow, Scotland, Jul. 2008, pp. 1-6.

[16] Y. Liu, B. Wang, and X. Zheng *et al*., "Fault location algorithm for non-homogeneous transmission lines considering line asymmetry," *IEEE Transactions on Power Delivery*, vol. 35, no. 5, pp. 2425-2437, Oct. 2020.

[17] S. Brahma and A. Girgis, "Fault location on a transmission line using synchronized voltage measurements," *IEEE Transactions on Power Delivery*, vol. 19, no. 4, pp. 1619-1622, Oct. 2004.

[18] C. Yu, L. Chang, and J. Cho, "New fault impedance computations for unsynchronized two-terminal fault location computations," *IEEE Transactions on Power Delivery*, vol. 26, no. 4, pp. 2879-2881, Oct. 2011.

[19] Y. Zhang, J. Liang, and Z. Yun *et al*., "A new fault-location algorithm for series-compensated double-circuit transmission lines based on the distributed parameter model," *IEEE Transactions on Power Delivery*, vol. 32, no. 6, pp. 2398–2407, Dec. 2017.

[20] F. Lopes, E. Leite Jr, and J. Ribeiro *et al*., "Single-ended multi-method phasor-based approach for optimized fault location on transmission lines," *Electric Power Systems Research*, vol. 212, Nov. 2022.

[21] X. Zhang, N. Tai, and P. Wu *et al*., "A new theory for locating line fault in power system: theoretical part," *IEEE Access*, vol. 7, pp. 91337-91346, Jul. 2019.

[22] Q. Wu, A. Bose, and C. Singh *et al*., "Control and stability of large-scale power system with highly distributed renewable energy generation: viewpoints from six aspects," *CSEE Journal of Power and Energy Systems*, vol. 9, no. 1, pp. 8-14, Jan. 2023.

[23] T. Wang, M. Jin, and Y. Li *et al*., "Adaptive damping control scheme for wind grid-connected power systems with virtual inertia control," *IEEE Transactions on Power Systems*, vol. 37, no. 5, pp. 3902-3912, Sept. 2022.

[24] G. Song, J. Suonan, and Q. Xu *et al*., "Parallel transmission lines fault location algorithm based on differential component net," *IEEE Transactions on Power Delivery*, vol. 20, no. 4, pp. 2396-2406, Oct. 2005.

[25] T. Lan, H. Xiao, and Y. Li *et al*., "Enhanced current differential protection for HVDC grid based on Bergeron model: a parameter error tolerable solution," *IEEE Transactions on Power Delivery*, vol. 36, no. 3, pp. 1869-1881, Jun. 2021.

[26] M. Davoudi, J. Sadeh, and E. Kamyab, "Transient-based fault location on three-terminal and tapped transmission lines not requiring line parameters," *IEEE Transactions on Power Delivery*, vol. 33, no. 1, pp. 179-188, Feb. 2018.

[27] F. Faria da Silva, "Comparison of Bergeron and frequency-dependent cable models for the simulation of

electromagnetic transients," in *2016 51st International Universities Power Engineering Conference (UPEC)*, Coimbra, Portugal, Nov. 2016, pp. 1-6.

[28] J. S and J. Luo, "Sinusoidal representation of a transient signal based on the hilbert transform," *Power System Protection and Control*, vol. 50, no. 1, pp. 1-7, Jan. 2022. (in Chinese)

[29] Z. Yin, G. Sun, and Z. Wei *et al*., "The research of fault section location for distribution network based on transient feature extraction and fuzzy clustering," in *2018 13th IEEE Conference on Industrial Electronics and Applications*, Wuhan, China, Jun. 2018, pp. 1279-1283.

[30] N. Giaquinto and A. Trotta, "Fast and accurate ADC testing via an enhanced sine wave fitting algorithm," *IEEE Transactions on Instrumentation and Measurement*, vol. 46, no. 4, pp. 1020-1025, Aug. 1997.

[31] Q. Zeng and D. Lu, "Curve and surface fitting based on moving leastsquares methods," *Journal of Engineering Graphics*, vol. 25, no. 1, pp. 84-89, 2004.

[32] J. Tao, M. Yu, and G. Chen *et al*., "Fundamental detection for a power system based on SWT", *Power System Protection and Control*, vol. 50, no. 18, pp. 39-49, Sept. 2022. (in Chinese)

[33] M. Karimi-Ghartemani and H. Karimi, "Analysis of symmetrical components in time-domain," in *48th Midwest Symposium on Circuits and Systems*, Covington, USA, Feb. 2005, pp. 28-31.

[34] J. Luo, K. Zhang, and T. Chen *et al*., "Distributed parameter circuit model for transmission line," in *2011 International Conference on Advanced Power System Automation and Protection*, Beijing, China, Apr. 2011, pp. 1529-1534.

[35] P. Chang, G. Song, and J. Hou *et al*., "A single-terminal fault location method for transmission lines integrated by inverter-type source," *IEEE Transactions on Power Delivery*, vol. 37, no. 3, pp. 1704-1713, Jun. 2022.

[36] M. Tang, H. Lu and B. Li, "Fault location of untransposed double-circuit transmission lines based on an improved Karrenbauer matrix and the QPSO algorithm," *Protection and Control of Modern Power Systems*, vol. 8, no. 1, pp. 44, Jan. 2023.